Nonlinear optical responses of multiply ionized noble gases: Dispersion and spin multiplicity effects

M. Tarazkar, D. A. Romanov, and R. J. Levis

Phys. Rev. A **94**, 012514 — Published 26 July 2016

DOI: 10.1103/PhysRevA.94.012514

Nonlinear Optical Responses of Multiply Ionized Noble Gases: Dispersion and Spin Multiplicity Effects

M. Tarazkar, [1,2] D. A. Romanov, [2,3] and R. J. Levis [1,2*]

[1]*Department of Chemistry, Temple University, Philadelphia, PA 19122*

[2]*Center for Advanced Photonics Research, Temple University, Philadelphia, PA 19122*

[3]*Department of Physics, Temple University Philadelphia, PA 19122*

Dynamic second-order hyperpolarizabilities of atomic noble gases and their multiply ionized ions are computed using *ab initio* multi-configurational self-consistent field cubic response theory. For each species, the calculations are performed at wavelengths ranging from the static regime to those about 100 nm above the first multi-photon resonance. The second-order hyperpolarizability coefficients progressively decrease as the electrons are removed from the system, in qualitative agreement with phenomenological calculations. In higher ionization states, the resulting nonlinear refractive index becomes less dispersive as a function of wavelength. At each ionization stage, the sign of the optical response depends on the number of electrons in the system and, if multiple state symmetries are possible, on the spin of the particular quantum state. Thus, for Ne^{+3} and Ne^{+4}, the hyperpolarizability coefficients in the low-spin states (^2P_u, and ^1S_g, respectively) are positive, while in the in high-spin states (^4S_u, and ^3P_g) they are negative. However, for doubly, triply, and quadruply charged Ar and Kr these coefficients do not undergo a sign change.

KEYWORDS: second-order hyperpolarizability, ionic hyperpolarizability, multiply ionized noble gases, degenerate four-wave mixing, nonlinear refractive index, multi-configurational self-consistent field level of theory

* rjlevis@temple.edu

I. INTRODUCTION

Understanding[1,2,3] and controlling[4,5] the nonlinear response of a medium to an intense laser pulse is important for a variety of phenomena including high-harmonic generation,[6,7,8] attosecond pulse formation,[9,10] and especially in laser filamentation.[11,12,13] The latter process results in coherent ultra-broadband radiation ranging from the UV to the far infrared (IR), with pulses as short as a few optical cycles being formed at long distances from the source (from the meter to kilometer scale).[14] Filaments are formed by a dynamic balance between self-focusing and defocusing effects induced by strong field ionization.[15] Predictive modeling of high-intensity laser pulses propagating in gas and/or ionized gas medium requires knowledge of linear and nonlinear optical responses of the neutral and ionized species. For laser intensities well below the atomic ionization threshold these responses are given by the induced polarization as determined by bound electrons.[16] For high-intensity laser pulses, where the population of ionized species is >10%, the contribution of each ionized atom/molecule to the nonlinear index of refraction must also be considered in nonlinear response.[8]

The effect of the external electric field on a medium may be given by the induced polarization $\boldsymbol{P}$, whose dependence on the electric field $\boldsymbol{F}$ at frequency ω can be expanded in a power series[16] as,

$$\begin{aligned} P(\omega) &= \chi^{(1)}(\omega)F(\omega) + \chi^{(3)}(\omega;\omega_1,\omega_2,\omega_3)\left|F(\omega)\right|^3 \\ &+ \chi^{(5)}(\omega;\omega_1,\omega_2,\omega_3,\omega_4,\omega_5)\left|F(\omega)\right|^5 + ... \end{aligned} \tag{1}$$

where $\chi^{(n)}$ is the *n*-th-order electric susceptibility of the material, $\sum_j \omega_j = \omega$, $\omega_j = \pm\omega$ and $\omega \geq 0$. Equation (1) implies the power expansion of the intensity-dependent refractive index,

$n(I) = n_0 + n_2 I + n_4 I^2 + \ldots$, where I is the intensity, n is the index of refraction, and n_{2j} coefficients are related to the $\chi^{(2n+1)}$ susceptibilities.

The Kerr self-focusing and self-phase modulation effects are described by the third-order susceptibility, $\chi^{(3)}$, in Eq. (1). The self-focusing is a key ingredient in the standard model of femtosecond laser filamentation, causing the collapse of the pulse and intense ionization.[17] The radially dependent negative index of refraction of the emerging plasma arrests the pulse collapse.[18] Alternatively, a fifth-order nonlinear susceptibility $\chi^{(5)}$ has been proposed to be negative and non-negligible, and thus responsible for defocusing strong field laser pulses. However, this so-called higher-order Kerr effect (HOKE)[19] hypothesis[20,21] has been experimentally[22 23,24,25] and theoretically[18, 26,27,28] ruled out in the relevant near-IR region. Once ionization occurs, the linear response of the free electrons typically dominates that of the bound electrons. However, the latter is responsible for the ongoing nonlinear dynamics.

In the process of laser filamentation and during the evolution of the filament wake channel, a large number of ions are generated in the gas medium, and their nonlinear optical properties may be expected to differ substantially from those of neutral species. The nonlinear response associated with ionization is manifest in a number of recent experiments, including bright higher harmonics generation in highly ionized gases,[8] polarization rotation in two-beam coupling settings,[29,30] igniter-heater processes in filament wake channels,[31] and giant Rabi sideband emission from the channels.[32,33] To make quantitative predictions of nonlinear optical characteristics of a substantially ionized gas medium, one needs to calculate nonlinear response of individual atomic and molecular ions.

Although several studies have been performed to investigate the nonlinear optical responses of neutral molecules/atoms,[34,35,36] fewer investigations have been performed for ions.[37,38] The limitations for ions arise from challenges in the numerical analysis of optical responses exhibited for open-shell systems[37,39] which are not encountered in closed-shell systems. The electron correlations in open-shell systems have been shown to play a critical role, and the presence of static and dynamic correlations further complicates the picture.[28]

Ab initio calculations of the nonlinear optical properties of neutral noble-gas atoms indicated the importance of using sufficiently large one-particle basis sets and applying high-level treatment of electron correlation.[40,36,41,42] For the second-order optical response of Ne, Ar, and Kr atoms, the coupled cluster singles and doubles (CCSD) electron correlation method along with the t-aug-cc-pV5Z basis set provides very good agreement between theory and experiment.[40,41,43] Based on these investigations, we calculated the fourth-order nonlinear response of atomic noble gases using the CCSD cubic response function along with the t-aug-cc-pV5Z[44,45] basis set for He, Ne, Kr, and with the q-aug-cc-pVQZ-pp basis set for Xe, and found that this approach provides a reasonable balance between computational time and accuracy.[26,27] To gain understanding of nonlinear responses in open-shell systems, we modified this approach by applying the multi-configurational self-consistent field (MCSCF) method, implemented in DALTON quantum chemistry package,[46] which we used to calculate the nonlinear response of nitrogen radical cation. [28] The open-shell electronic system of N_2^+ was found to exhibit negative second-order optical nonlinearity, with the values of the hyperpolarizability coefficient, $\gamma^{(2)}$, being about an order of magnitude greater than those of neutral N_2,. The large value of the ionic nonlinearity indicates an enhanced role of excitations in the polarization response of ion as

compared with the neutral molecule. We used the same methodology to calculate quadratic and quartic refractive indices of multiply ionized Ar at 270 nm wavelength.[8]

In this paper, we report the results of a systematic study of the dynamic linear and nonlinear responses of multiply ionized atoms in a series of noble gases, He, Ne, Ar, Kr, and Xe, for wavelengths ranging from the UV to the IR. The *ab initio* calculations are conducted using the MCSCF method, implemented in DALTON quantum chemistry package.[46] For optimization, various active spaces are tested through the computation of the degenerate four-wave mixing (DFWM) nonlinear coefficient at 800 nm wavelength for each ionized species to determine convergence of the calculations. The method is benchmarked by comparison with the results of CCSD-based calculations for the cases of neutrals and sextuply-charged ions, where the latter approach is applicable for closed-shell systems. Then, we consider the effects of spin state on nonlinear optical responses. Finally, the dispersion curves for the degenerate four-wave mixing coefficient, which determines $n_2(\omega)$, are obtained for each of the noble gases in various ionization state.

The paper is organized as follows. In Section II, we explain the methodology, outline the convergence tests, and discuss the active-space optimization. In Section III, we report on the active-space choice and the benchmarking, discuss spin multiplicity effects on the DFWM coefficient for multiply ionized noble gases, and present the dispersion curves of the DFWM coefficient for multiply-charged ions of each of the noble gases, in most stable ionic configuration, in a frequency range from UV to IR. Concluding remarks are presented in Section IV.

II. THEORETICAL METHODOLOGY

The open-shell electronic configuration of the noble-gas ions precludes calculation of the dynamic nonlinear response using coupled-cluster (CC) theory[47] in the DALTON quantum chemistry package.[46] To overcome this limitation, the MCSCF level of theory is used to calculate the dynamic (hyper)polarizability coefficients for multiply ionized noble gas atoms. The optical responses for multiply ionized noble gases were calculated with the t-aug-cc-pV5Z basis set to provide a reasonable balance between computation time and accuracy.[26,27]

The response of an atom or molecule to a time-dependent electric field, $\mathbf{F} = \mathbf{F}_0 + \mathbf{F}_\omega \cos(\omega t)$ is approximated following the expansion of the induced dipole moment as a function of instantaneous field magnitude,[48]

$$\begin{aligned}
\mu_\lambda &= \mu_\lambda^0 + \alpha_{\lambda\mu}(0;0)F_{0\mu} + \alpha_{\lambda\mu}(-\omega;\omega)F_{\omega\mu}\cos(\omega t) + \frac{1}{2}\beta_{\lambda\mu\nu}(0;0,0)F_{0\mu}F_{0\nu} \\
&+ \frac{1}{4}\beta_{\lambda\mu\nu}(0;\omega,-\omega)F_{\omega\mu}F_{\omega\nu} + \beta_{\lambda\mu\nu}(-\omega;0,\omega)F_{0\mu}F_{\omega\nu}\cos(\omega t) \\
&+ \frac{1}{4}\beta_{\lambda\mu\nu}(-2\omega;\omega,\omega)F_{\omega\mu}F_{\omega\nu}\cos(2\omega t) \\
&+ \frac{1}{6}\gamma_{\lambda\mu\nu\rho}{}^{(2)}(0;0,0,0)F_{0\mu}F_{0\nu}F_{0\rho} + \frac{1}{2}\gamma_{\lambda\mu\nu\rho}{}^{(2)}(-\omega;\omega,0,0)F_{\omega\mu}F_{0\nu}F_{0\rho}\cos(\omega t) \\
&+ \frac{1}{8}\gamma_{\lambda\mu\nu\rho}{}^{(2)}(-\omega;\omega,-\omega,\omega)F_{\omega\mu}F_{\omega\nu}F_{\omega\rho}\cos(\omega t) \\
&+ \frac{1}{4}\gamma_{\lambda\mu\nu\rho}{}^{(2)}(-2\omega;\omega,\omega,0)F_{\omega\mu}F_{\omega\nu}F_{0\rho}\cos(2\omega t) \\
&+ \frac{1}{4}\gamma_{\lambda\mu\nu\rho}{}^{(2)}(0;\omega,-\omega,0)F_{\omega\mu}F_{\omega\nu}F_{0\rho} + \frac{1}{24}\gamma_{\lambda\mu\nu\rho}{}^{(2)}(-3\omega;\omega,\omega,\omega)F_{\omega\mu}F_{\omega\nu}F_{\omega\rho}\cos(3\omega t) + \ldots
\end{aligned} \tag{2}$$

where the subscripts (λ, μ, etc.) relate to the Cartesian coordinates in atomic or molecular axes on which the external field is projected. The nonlinear optical effects, associated with the second-order hyperpolarizability coefficients $\gamma^{(2)}_{\lambda\mu\nu\rho}$, include DC-Kerr, $\gamma^{DC-Kerr}_{\lambda\mu\nu\rho}(\omega) = \gamma^{(2)}_{\lambda\mu\nu\rho}(-\omega;\omega,0,0)$,

electric field-induced second-harmonic generation, $\gamma^{ESHG}_{\lambda\mu\nu\rho}(\omega) = \gamma^{(2)}_{\lambda\mu\nu\rho}(-2\omega;\omega,\omega,0)$, and degenerate four wave mixing, $\gamma^{DFWM}_{\lambda\mu\nu\rho}(\omega) = \gamma^{(2)}_{\lambda\mu\nu\rho}(-\omega;\omega,-\omega,\omega)$. The latter coefficient is related to the nonlinear refractive index, n_2.

To address possible comparisons with experimental response of the medium, the mean hyperpolarizability coefficients should be considered, which are given by isotropic average of $\gamma^{(2)}$. A quantum state of the electronic system of an ion can have even or odd symmetry, and the mean hyperpolarizability coefficients are different in these two cases (see Eqs. 3 and 4 below). Specifically, for a single-configuration orbital occupation,[46,49] the parity is determined by $\sum_i l_i$, where the sum is over all unpaired electrons and l_i is the orbital angular momentum of the i^{th} electron. Hence the ns^2np^3 occupation of a triply ionized noble gas atom gives rise to three odd-parity states: ^4S_u, ^2D_u, and ^2P_u, whereas the ns^2np^4 (or ns^2np^2) occupation of a doubly (or quadruply) ionized noble gas atom yields even-parity states: ^3P_g, ^1D_g, and ^1S_g.[50,51] These state symmetries are obtained based on Pauli's principle, where half-integer spin (s=1/2, 3/2, …) requires an anti-symmetric wavefunction, and integer spins (s=0, 1,…) corresponds to a symmetric wavefunction.[52] For neutral noble-gas atoms, the ground-state symmetry is S, and the average $\gamma^{(2)}$ values are determined as,

$$\gamma^{(2)}_{\parallel} = \gamma^{(2)}_{zzzz}. \tag{3}$$

For the ionized atoms with P ground-state symmetry the (hyper)polarizability depends on the absolute value of the orbital angular momentum quantum number $|M_L|$, and thus separate

calculations are needed for $|M_L| = 0$ (corresponding to $\gamma^{(2)}_{xxxx}$) and $|M_L| = 1$ (corresponding to $\gamma^{(2)}_{zzzz}$) states.[37] Then, the mean (hyper)polarizability for a P-state is determined as,[37]

$$\gamma^{(2)}_{\text{II}} = (\gamma^{(2)}_{xxxx} + 2\gamma^{(2)}_{zzzz}) / 3. \quad (4)$$

In MCSCF response theory[53,54], a key step is the construction of appropriate active space. The configuration spaces are chosen based on second-order Møller–Plesset perturbation theory (MP2) natural orbital (NO) occupation numbers.[49] The core orbitals have MP2 NO occupancies close to two, while the deviations from two become more pronounced for the valence orbitals. The unoccupied orbitals have small occupancies which decrease toward zero for higher-energy orbitals.[49] Typically, the active space includes orbitals with occupations greater than 0.005, as well as the orbitals with occupations lower than 1.995.[55] However, additional careful consideration is often recommended as to which orbitals should be ruled inactive.[56,57] We will use the designation (*n*,*m*) to represent an active space of *n* electrons in *m* orbitals.

Table 1 displays the MP2 NO occupations for neutral He, Ne, Ar, and Kr atoms and their evenly-charged ions. In the DALTON program, perturbation theory on UHF reference wavefunction (MP2 method) doesn't work for open-shell systems, which for the systems of study correspond to atoms/ions with P symmetries. Thus, the S symmetry is considered for the calculations of NO occupations for doubly and quadruply ionized systems. Once the active spaces for evenly-charged ions were determined, the odd-charged ions follow the same active spaces as the nearest even-charged ion that has more electrons. Table 1 shows that, a reasonable active space for neutral He consists of two electrons in two *s* orbitals and one *p* orbital (2,5). For neutral Ne, the active space partitions eight electrons in three *s* and two *p* orbitals (8,9). To determine the convergence of the DFWM coefficient, the calculations were also performed with

the active spaces of (8,12) and (8,17). Similarly, for neutral Ar, the active space is formed by partitioning eight electrons into two *s*, two *p* and one *d* orbitals (8,13). Here, we also performed the calculations with the active spaces enlarged to three *s* orbitals (8,14) or four *s* orbitals (8,15). For neutral Kr, the active space partitions the eight valence electrons into two *s*, two *p* and one *d* orbitals (8,13), and an extended active space including two *s*, two *p* and two *d* orbitals (8,18) was also tested.

TABLE I. Natural orbital occupation numbers calculated with MP2 wavefunction, for He, Ne, Ar, and Kr atoms and ions. The occupations larger than 0.0001 are listed.

Orbital number	***s***	p_x	p_y	p_z	d_{xy}	d_{xz}	d_{yz}	d_{x2-y2}	d_{z2}
	s		*P*				*D*		
He									
1	1.98875		0.00179						
2	0.00472		0.00010						
3	0.00014								
Ne									
1	1.99938		1.97875				0.00394		
2	1.99004		0.01290				0.00040		
3	0.00712		0.00010						
Ne^{+2}									
1	1.99942		1.98596*				0.00256		
2	1.98451		0.00467				0.00023		
3	0.00321		0.0003						
Ne^{+4}									
1	1.99947		1.98710				0.00227		
2	1.97643		0.00184						
3	0.00144		0.00019						
4	0.00079								
Ne^{+6}									
1	1.99956		0.01183				0.00012		
2	1.96338								
3	0.00031								
Ar									
1	1.99992		1.99777				0.01765		
2	1.99907		1.95981				0.00101		

3	1.98442	0.00816	0.00051
4	0.00550	0.00088	0.00026
5	0.00066	0.00015	
Ar^{+2}			
1	1.99993	1.99788	0.01304
2	1.99911	<u>1.96450</u>	0.00082
3	1.97217	0.00383	
4	0.00437	0.00112	
5	0.00274	0.00069	

* The non-degenerate occupations for particular angular momentums are denoted with an underline.

TABLE I. (Continued) Natural orbital occupation numbers calculated with MP2 wavefunction, for He, Ne, Ar, and Kr atoms and ions. The occupations larger than 0.0001 are listed.

Orbital number	***s***	***p_x***	***p_y***	***p_z***	***d_{xy}***	***d_{xz}***	***d_{yz}***	***d_{x2-y2}***	***d_{z2}***
	s		*P*				*D*		
Ar^{+4}									
1	1.99992		1.99801				0.00950		
2	1.99916		<u>1.96648</u>				0.00070		
3	1.96468		0.00212						
4	0.00535		0.00065						
5	0.00152								
Ar^{+6}									
1	1.99992		1.99770				0.00101		
2	1.99925		0.01059				0.00038		
3	1.96539		0.00056						
4	0.00084								
Kr									
1	1.99999		1.99991				1.99462		
2	1.99995		1.99788				0.01833		
3	1.99869		1.96029				0.00314		
4	1.98335		0.00802				0.00047		
5	0.00589		0.00173						
6	0.00115								
Kr^{+2}									
1	1.9999995		1.99991				1.99477		
2	1.9999512		1.99744				0.01251		
3	1.9987352		<u>1.96463</u>				0.00247		
4	1.9720237		0.00477				0.00026		
5	0.0063636		0.00099						
6	0.0017033								
Kr^{+4}									

1	1.99999	1.99991	1.99501
2	1.99995	1.99813	0.00434
3	1.99879	1.96659	0.00046
4	1.96591	0.00354	
5	0.00702	0.00119	
6	0.00274		
7	0.00168		
Kr^{+6}			
1	1.99999	1.99991	1.99539
2	1.99995	1.99761	0.00401
3	1.99885	0.01073	0.00027
4	1.96717	0.00144	
5	0.00215		

III. RESULTS AND DISCUSSION

A. Active-space optimization and benchmarking

To date there are no direct measurements of linear and nonlinear optical properties of ions to use as benchmark. Thus, in present study, the performance of the MCSCF method for the calculation of second-order nonlinear optical responses of multiply ionized noble gases is benchmarked by comparing the calculated coefficients at 800 nm with those computed with CCSD theory. This comparison is performed for neutral atomic noble gases and the sextuply ionized species, which are within the limits of applicability of CCSD model. The DFWM coefficient for each ionized species is also calculated at 800 nm as a function of active space in order to analyze the convergence of the second-order nonlinear responses in the MCSCF method.

Figure 1 shows that the DFWM coefficients have approximately the same value at 800 nm for He atom calculated with MCSCF (~44.0 a.u.) and CCSD (~44.3 a.u.) methods. Calculations for singly ionized He are performed by partitioning one electron into two *s* and one *p* orbitals. The figure displays the decrease of nonlinear response for singly ionized He to ~1.3

a.u., which is attributed to the decrease in electron density as well as the increased interaction between the remaining electron and the nucleus.

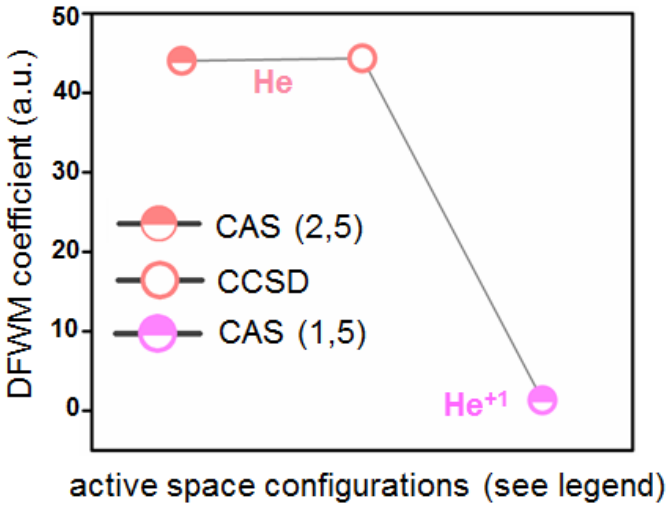

FIG. 1. (Color online) The DFWM coefficient for neutral He and He^{+1} at 800 nm. For neutral atom, the calculations were performed using both CCSD and MCSCF methods, and for the ion, using MCSCF. The t-aug-cc-pV5Z basis set was used in all calculations.

Figure 2 summarizes the results of second-order hyperpolarizability coefficients for Ne and its multiply ionized species at 800 nm, studied with different active spaces. To test whether the active space of three *s* and two *p* orbitals (8,9) for Ne atom is sufficient to perform the nonlinear response calculations, we follow the calculations with enlarged active space i.e., (8,12) with inclusion of eight electrons in three *s* orbitals and three *p* orbitals, and/or (8,17) with inclusion of eight electrons in three *s*, three *p*, and one *d* orbitals. Comparison of the results reveals agreement among MCSCF (using different active spaces), CCSD model and experimental measurements[58] within ~2%. As mentioned in Section II orbital occupation values lower than 0.005 suggest exclusion from the active space,[55] however, for the cases studied here, some orbital occupation numbers are lower but close to 0.005. Given that selecting active spaces in a molecule/atom depends on various parameters,[55] we tested different active spaces for each

species or ion by adding or subtracting orbitals that have occupations close to each other and/or close to 0.005. Note that large gaps in the occupation numbers are used as a means to choose which orbitals are not required to be included in the active space. The results for Ne and neon ions are shown in Figure 2. In general, the larger active spaces do not result in markedly different values for the second order-hyperpolarizability.

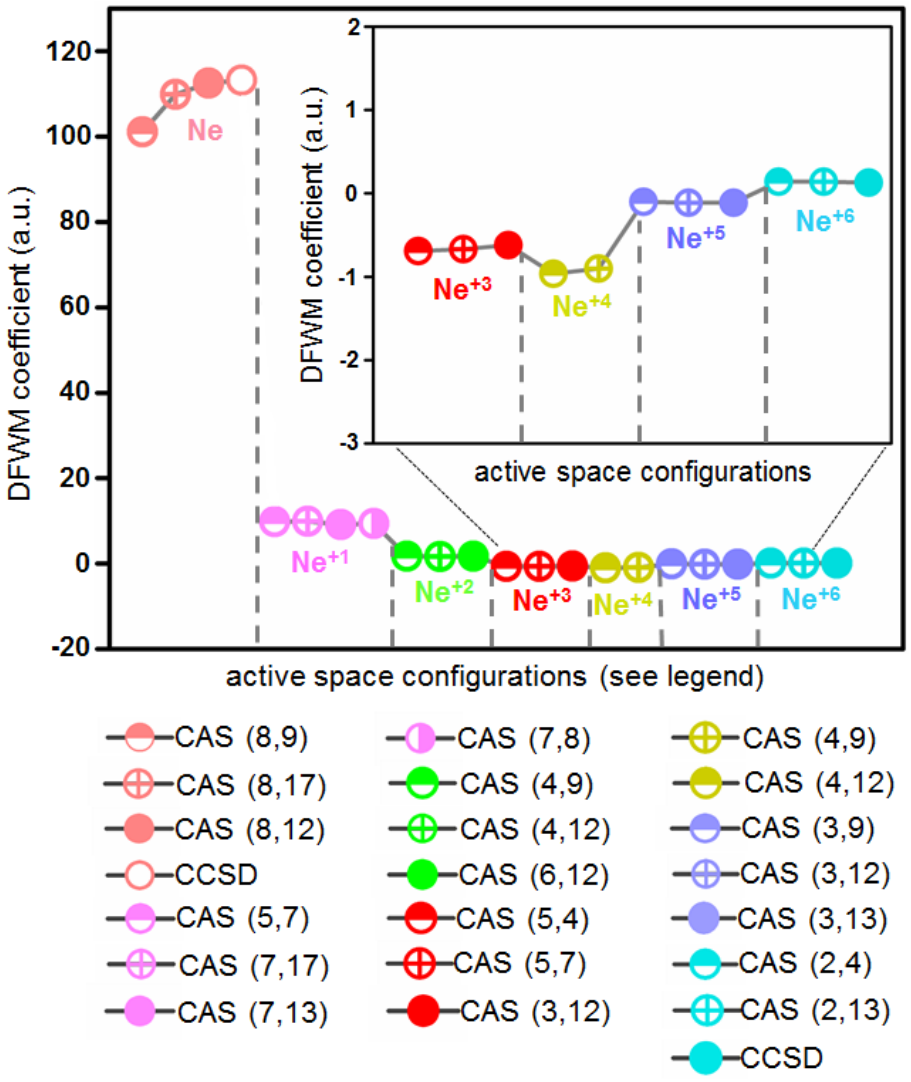

FIG. 2. (Color online) The DFWM coefficient for Ne atom and ions at 800 nm as a function of active space size. For neutral Ne and for Ne^{+6}, the calculations were performed using both CCSD and MCSCF methods, for the rest of the ions, MCSCF approach was used. The symmetries used for calculations of Ne, Ne^{+1}, Ne^{+2}, Ne^{+3}, Ne^{+4}, Ne^{+5}, and Ne^{+6} are ^1S_g, ^2P_u, ^3P_g, ^4S_u, ^3P_g, ^2P_u, and ^1S_g, respectively. The t-aug-cc-pV5Z basis set was used in all calculations.

Figure 3 reveals the DFWM values calculated at 800 nm for neutral argon and the corresponding multiply ionized species. For the case of Ar, as discussed in Section II, the occupations of natural orbitals suggest partitioning eight electrons in two *s*, two *p* and one *d* orbitals (8,13). The enlarged active spaces (8,14) and/or (8,15) were considered as well.

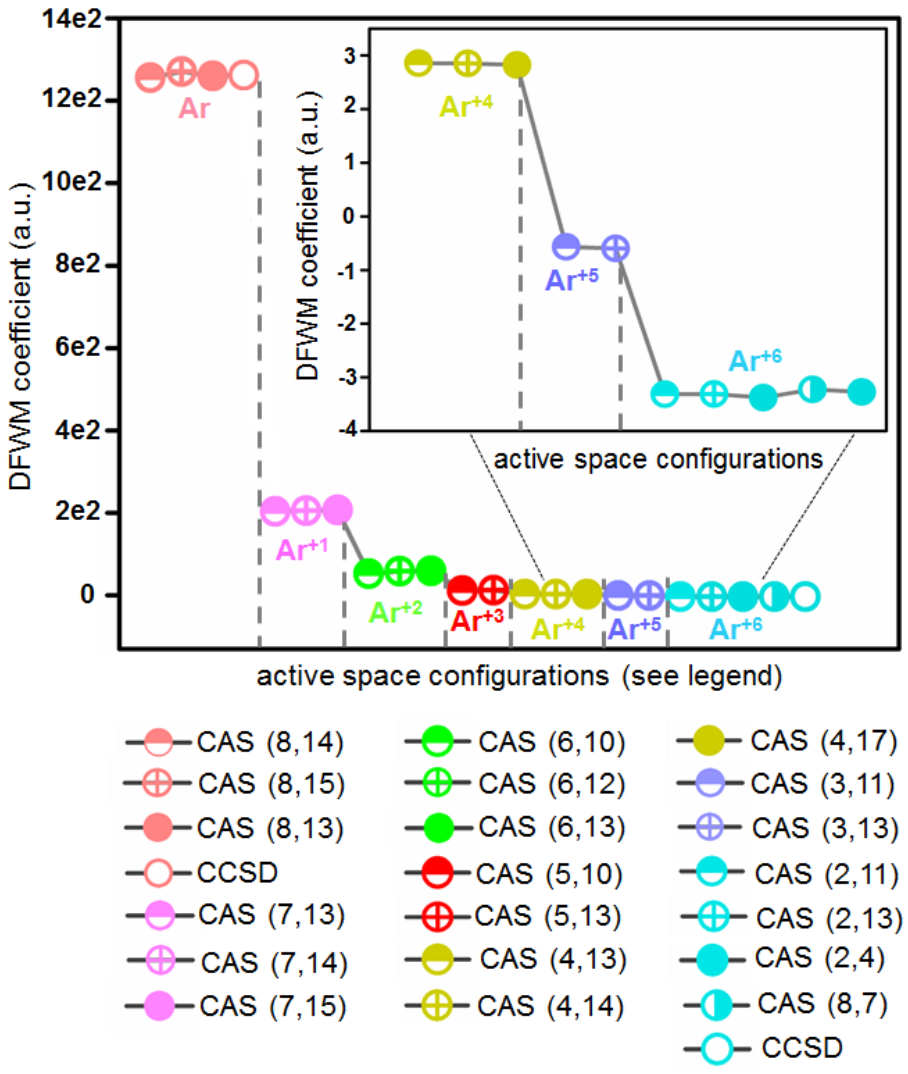

FIG. 3. (Color online) The DFWM coefficient for Ar atom and ions at 800 nm as a function of active space size. For neutral Ar and for Ar^{+6}, the calculations were performed using both CCSD and MCSCF methods, for the rest of the ions, MCSCF approach was used. The symmetries used for calculations of Ar, Ar^{+1}, Ar^{+2}, Ar^{+3}, Ar^{+4}, Ar^{+5}, and Ar^{+6} are ^1S_g, ^2P_u, ^3P_g, ^4S_u, ^3P_g, ^2P_u, and ^1S_g, respectively. The t-aug-cc-pV5Z basis set was used in all calculations.

The corresponding results indicate an agreement among various active spaces in MCSCF method, which are also consistent with CCSD calculations and the experimental measurements,[59,58] confirming the appropriate choice of active space. Similar benchmark studies have been performed for multiply ionized argon. The results indicate that the deviations of DFWM values calculated using different active spaces are ≤ 5% (see Fig. 3).

Figure 4 displays the calculations for Kr and its multiply ionized species at 800 nm. The occupation numbers of natural orbitals for Kr atom, suggest assignment of the eight electrons to two *s*, two *p*, and one *d* orbitals (8,13) with possible enlargement of the active space by adding one set of *d* orbitals (8,18), as discussed in Section II. The difference of DFWM at 800 nm calculated with two active spaces for neutral Kr atom is ≤1% and the difference between the second-order hyperpolarizability coefficients calculated using MCSCF model and CCSD method is less than ~3%, which confirms the appropriate choice of active spaces. The benchmark studies for multiply ionized krypton are shown in Figure 4. The corresponding DFWM coefficients reveal that the larger active spaces do not result in remarkable change in the second order-hyperpolarizability coefficients. The detailed analysis of active spaces, for the calculations of second-order nonlinear responses of each ionized noble gases, can be found in Supplementary Materials.

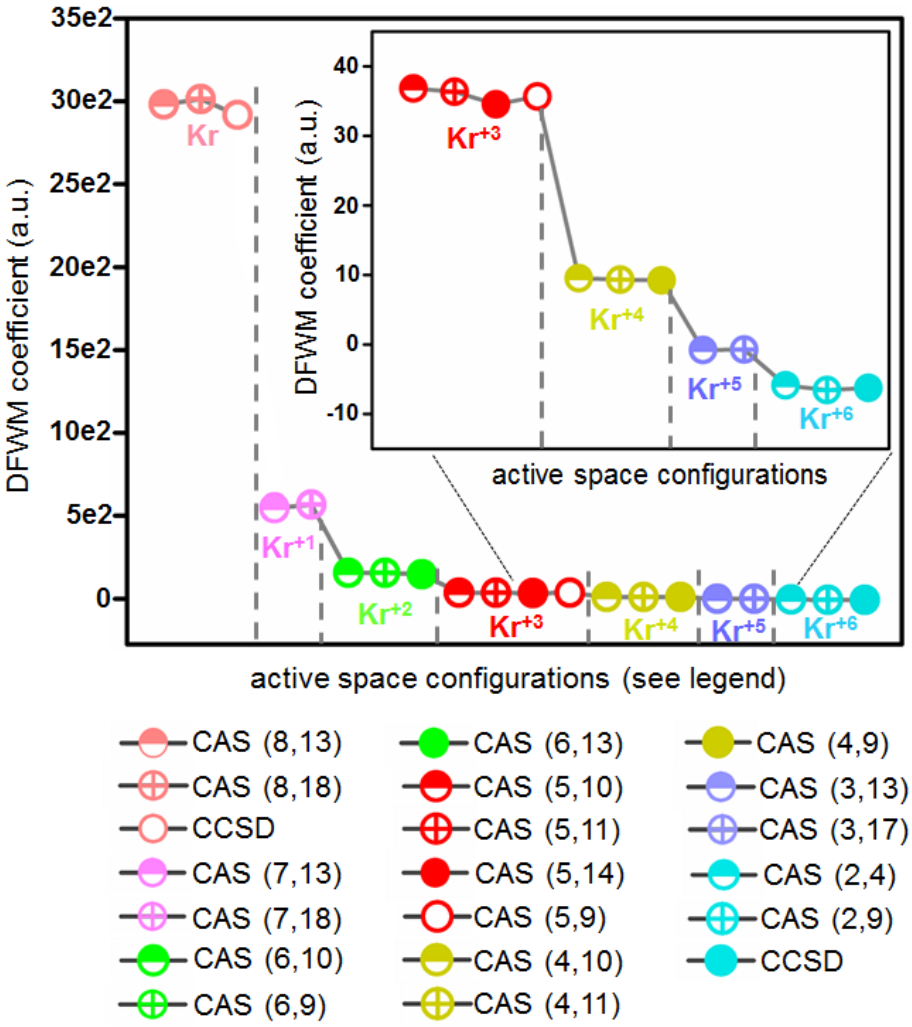

FIG. 4. (Color online) The DFWM coefficient for Kr atom and ions at 800 nm as a function of active space size. For neutral Kr and for Kr^{+6}, the calculations were performed using both CCSD and MCSCF methods, for the rest of the ions, MCSCF approach was used. The symmetries used for calculations of Kr, Kr^{+1}, Kr^{+2}, Kr^{+3}, Kr^{+4}, Kr^{+5}, and Kr^{+6} are ^1S_g, ^2P_u, ^3P_g, ^4S_u, ^3P_g, ^2P_u, and ^1S_g, respectively. The t-aug-cc-pV5Z basis set was used in all calculations.

B. Spin multiplicity effects of the DFWM for multiply ionized noble gases

As discussed in Section II, an atom can possess various state symmetries depending on the configuration of the valence orbital occupations. In present study, different symmetries allowed by quantum mechanics are investigated to inspect the effect of spin multiplicity on the DFWM optical responses. We initially consider the symmetries for Ne^{+n} ($1 \leq n \leq 6$), subsequently

generalize the results to all ionized noble gases that have the same valence electronic configurations. For atoms/ions such as Ne, Ne^{+1}, Ne^{+5}, and Ne^{+6} (with valence electronic configurations $2s^2\,2p^6$, $2s^2\,2p^5$, $2s^2\,2p^1$, and $2s^2$, respectively) only one symmetry is defined; for Ne and Ne^{+6} the ground state symmetry is ^1S_g, while for Ne^{+1} and Ne^{+5} the symmetry is defined as ^2P_u. For the ions of Ne^{+2}, Ne^{+3}, and Ne^{+4} (with valence electronic configuration $2s^2\,2p^4$, $2s^2\,2p^3$, and $2s^2\,2p^2$, respectively) more than one symmetry can be defined. For Ne^{+2} and Ne^{+4} the ground state symmetries are defined as ^3P_g and ^1S_g, while for Ne^{+3} the symmetries are defined as ^2P_u and ^4S_u.

Figures 5-7 display the $\gamma_{\lambda\mu\nu\rho}(-\omega;\omega,-\omega,\omega)$ optical response for ionized Ne, Ar, and Kr at 800 nm, including defined symmetries for each ionized species. As can be seen in Fig. 5, the magnitude and sign of nonlinear optical response for Ne^{+n} depends on the state symmetry applied in the calculations. For Ne^{+2}, the optical response is positive at both symmetries and the calculated values are in close agreement with each other. In contrast, for the case of Ne^{+3} the nonlinear response coefficients exhibit positive and negative signs depending on the symmetry of the system. The high–spin state (^4S_u) has a negative sign of $\gamma_{\lambda\mu\nu\rho}(-\omega;\omega,-\omega,\omega)$ and the low-spin state (^2P_u) holds a positive sign of DFWM coefficient. The same trend is observed for quadruply charged Ne, where the high-spin state (^3P_g) corresponds to negative value of DFWM response and low-spin state (^1S_g) results in positive nonlinear response. These calculations suggest that nonlinear optical responses may be controlled via manipulating the spin state of the system.

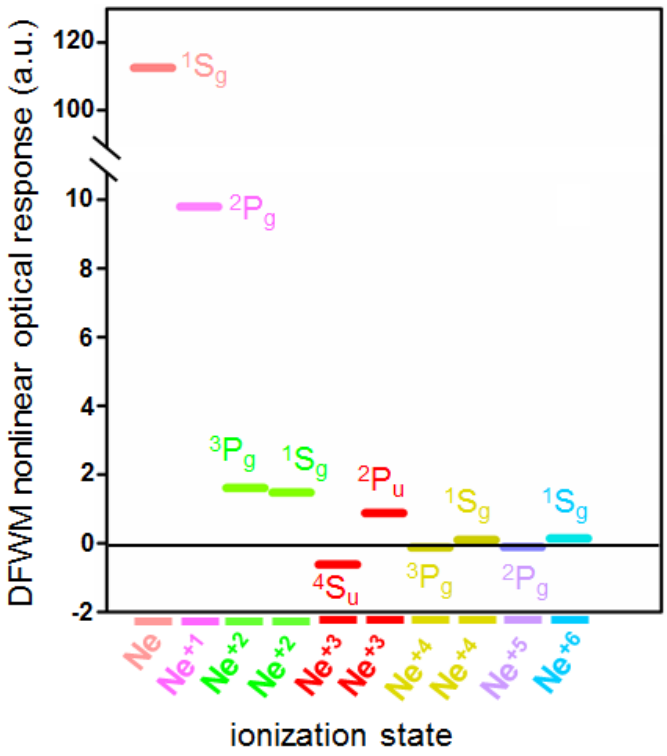

FIG. 5. (Color online) The DFWM coefficient for neutral Ne atom and ions at 800 nm, calculated for the various allowed symmetries. The calculations were performed using CAS (8,12), CAS (5,7), CAS (4,12), CAS (3,12), CAS (4,13), CAS (3,13), and CAS (2,4) for Ne, Ne^{+1}, Ne^{+2}, Ne^{+3}, Ne^{+4}, Ne^{+5}, and Ne^{+6}, respectively.

For the cases of multiply charged Ar and Kr, the sign of the nonlinear optical response does not change by varying the symmetry of the system (see Figs. 6 and 7) which may be due to negligible energy differences between two symmetries in ionic species of Ar and Kr. In contrast, for Ne^{+n}, $2 \leq n \leq 4$, the energy differences between two symmetries is remarkable. For doubly ionized Ar, the absolute values of DFWM second-order nonlinear coefficients for high- and low-spin states vary from ~52 to ~61 a.u., respectively. Moreover, for triply ionized Ar the value of the $\gamma_{\lambda\mu\nu\rho}(-\omega;\omega,-\omega,\omega)$ coefficient at 800 nm shifts from ~12 a.u. for the ion at high spin-state, to ~18 a.u. for the ion at low-spin state. For Ar^{+4} the DFWM coefficient at 800 nm slightly varies

from the value of ~2.8 a.u., for the ion with ^3P_g symmetry, to 2.4 a.u., for the ion with ^1S_g symmetry (see Fig. 6). Comparison of the nonlinear coefficients of Kr ions at 800 nm, obtained

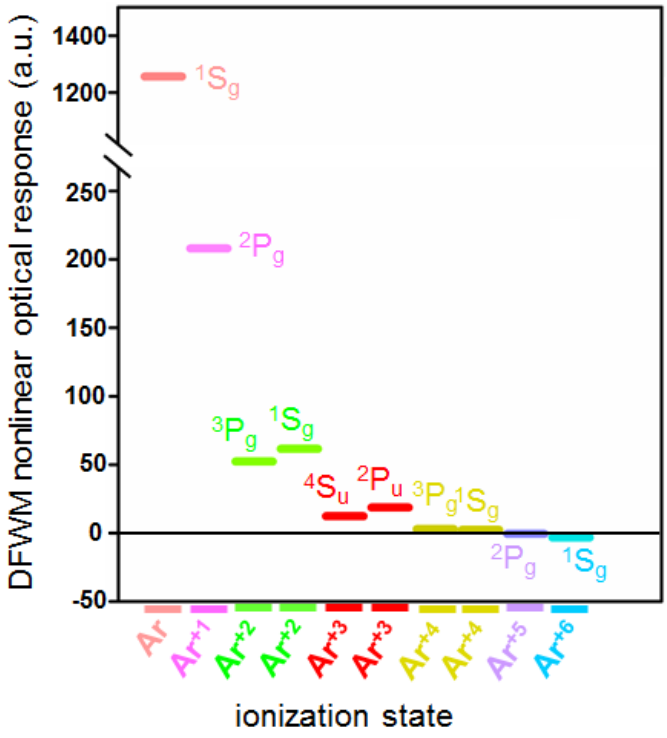

FIG. 6. (Color online) The DFWM coefficients for neutral Ar atom and ions at 800 nm, calculated for the various allowed symmetries. The calculations were performed using CAS (8,14), CAS (7,14), CAS (6,10), CAS (5,13), CAS (4,13), CAS (3,13), and CAS (2,13) for Ar, Ar^{+1}, Ar^{+2}, Ar^{+3}, Ar^{+4}, Ar^{+5}, and Ar^{+6}, respectively.

using different state symmetries, demonstrates a change in DFWM of doubly ionized Kr from ~156 a.u. to ~126 a.u for the ion with ^3P_g and ^1S_g symmetries, respectively. For triply ionized Kr this value varies from ~37 a.u. to ~40 a.u. for high and low spin-states, respectively. Finally for Kr^{+4} the DFWM second-order nonlinear coefficient is separated from ~9.2 a.u. for the ion with ^3P_g symmetry, to ~8.5 a.u. for the ion with ^1S_g symmetry (see Fig. 7).

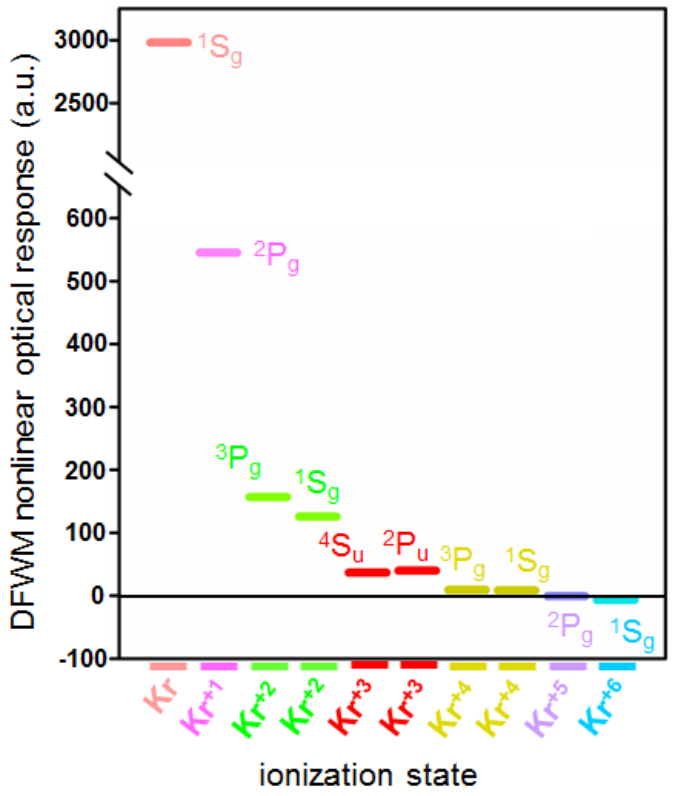

FIG. 7. (Color online) The DFWM coefficients for neutral Kr atom and ions at 800 nm, calculated for the various allowed symmetries. The calculations were performed using CAS (8,13), CAS (7,13), CAS (6,10), CAS (5,10), CAS (4,9), CAS (3,13), and CAS (2,9) for Kr, Kr^{+1}, Kr^{+2}, Kr^{+3}, Kr^{+4}, Kr^{+5}, and Kr^{+6}, respectively.

C. Dispersion of the DFWM for multiply ionized noble gases in a frequency range from UV to IR

Given that the preliminary MCSCF calculations of multiply ionized argon[8] at wavelength of 270 nm showed a reasonable agreement with both measurement[8,60] and the TDSE calculations, and the second-order nonlinear responses for multiply ionized species as a function of active space appears to have converged, the method presented here has been validated. We proceed to determine the DC-Kerr, ESHG, and DFWM optical responses for a wide range of frequencies ranging from 100 nm above the lowest order multi-photon absorption resonance to the static regime using the approach outlined in Section II.

Figures 8-11 display the variation of DFWM coefficients versus wavelength, ranging from ~100 nm above the first multi-photon resonance to the static regime, for multiply charged noble gases obtained from CAS (2,5) for He, CAS (1,5) for He^{+1}, CAS (8,12) for Ne, CAS (5,7) for Ne^{+1}, CAS (4,12) for Ne^{+2}, CAS (3,12) for Ne^{+3}, CAS (4,13) for Ne^{+4}, CAS (3,13) for Ne^{+5}, CAS (2,4) for Ne^{+6}, CAS (8,14) for Ar, CAS (7,14) for Ar^{+1}, CAS (6,10) for Ar^{+2}, CAS (5,13) for Ar^{+3}, CAS (4,13) for Ar^{+4}, CAS (3,13) for Ar^{+5}, CAS (2,13) for Ar^{+6}, CAS (8,13) for Kr, CAS (7,13) for Kr^{+1}, CAS (6,10) for Kr^{+2}, CAS (5,10) for Kr^{+3}, CAS (4,9) for Kr^{+4}, CAS (3,13) for Kr^{+5}, and CAS (2,9) for Kr^{+6}. The symmetries used for wavelength dispersion of DFWM coefficients for M, M^{+1}, M^{+2}, M^{+3}, M^{+4}, M^{+5}, and M^{+6} are ^1S_g, ^2P_u, ^3P_g, ^4S_u, ^3P_g, ^2P_u, and ^1S_g respectively, where M^{+n} corresponds to Ne, Ar, and/or Kr ions. The DC-Kerr and ESHG responses at different wavelengths are shown in Tables S1-S4 in Supplemental Materials.

D. Interpreting the DFWM coefficient as a function of charge state

Comparison of the DFWM coefficients calculated for multiply ionized noble gases indicates a general decrease in the optical response of ionized species in comparison with neutral systems, suggesting that the increasing electron density plays a crucial role for enhancing the nonlinear responses of the atoms/molecules.[61] This trend may be rationalized as a manifestation of two related effects. Upon ionization, the number of electrons responding to the optical field is decreased and thus decreases polarizability. In addition, when a system is ionized, the screening effect of the electrons is reduced, thus the remaining electrons are bound more tightly to the nucleus, becoming less responsive to external fields.

Single ionization of He decreases the DFWM nonlinear optical response by a factor of 33 as compared with that of neutral He atom (see Fig. 8). For the case of Ne, the DFWM optical response of singly charged system decreased by a factor of ~11 in comparison with neutral atom,

and for sextuply ionized Ne the nonlinear response decreases by two orders of magnitude in comparison with Ne atom. Surprisingly, the decrease of the DFWM value with increasing ionization state in Ne is not monotonic: the singly, doubly, triply and quadruply ionized Ne decreases the quadratic Kerr coefficient, but the quintuply and sextuply ionized states of Ne display an increase in the Kerr coefficient (see Fig.9). Removing one electron from neutral Ar atom decreases the DFWM optical response by a factor of ~6 in comparison with atomic argon. At each sequential ionization state the nonlinear properties decreases uniformly, with the sextuply ionized species having a DFWM coefficient that is two orders of magnitude smaller than that of the neutral atomic argon (see Fig.10). Similarly, for Kr^{+1} the DFWM optical response decreases by a factor of ~5 in comparison with that of the neutral atom; removing six electrons from the neutral atom, the DFWM coefficient diminishes by two orders of magnitude in comparison with Kr atom (see Fig.11). Note that the quadratic nonlinear index of refraction relates to DFWM through[62],

$$n_2(\frac{cm^2}{W}) = 8.28\times10^{-23}\gamma^{(2)}_{DFWM}(a.u.). \quad (5)$$

So the discussions based on DFWM coefficient corresponds to the n_2 quadratic nonlinear index of refraction and Kerr effect, as they are linearly related.[28]

In Figs. 8-11, the decrease in index of refraction for singly ionized noble gases, as compared with their neutral atoms, can be attributed to the differences in the ionization potentials (IP). The IP for helium, neon, argon and krypton are 24.6, 21.5, 15.7, 14.0 eV, respectively, and the IP rises to 54.4, 44.4, 27.6, and 24.2 eV for the corresponding singly ionized species. Thus, a smaller number of infrared photons are required to effect multiphoton ionization of neutral noble gas atoms, in comparison with their singly ionized species. The increase in ionization potential reduces the resulting nonlinear refractive index values, which can be explained by the Kramers-

Kronig (KK) formalism[63,64] indicating that the nonlinear refraction coefficient n_{2k} is related to the (k+1) number of photons required to reach the ionization potential, as illustrated by the transition from krypton to helium neutral atoms, where the n_2 at 800 nm for He is calculated to be 3.64×10^{-9} cm^2/TW and for Kr the n_2 increases to 2.46×10^{-7} cm^2/TW.[27]

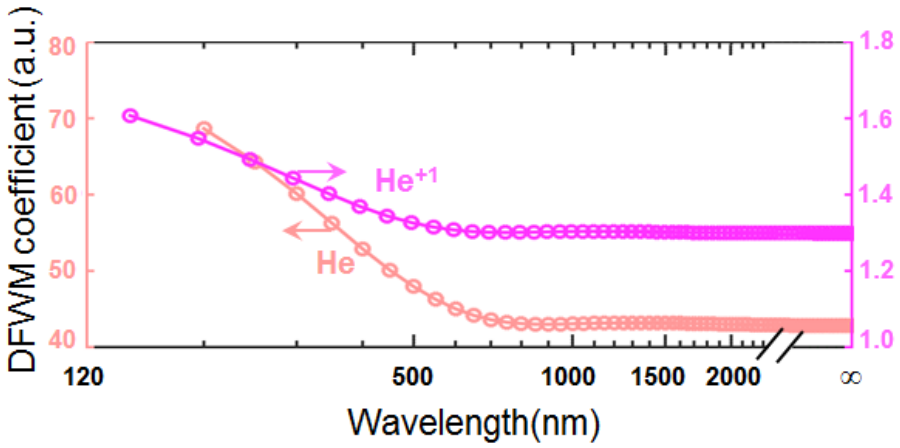

FIG. 8. (Color online) The DFWM coefficient for He and He^{+1} versus wavelength ranging from ~100 nm above the first multi-photon resonance to the static regime. The calculations were performed using CAS (2,5) for He and CAS (1,5) for He^{+1}.

The phenomenological calculations based on the nonlinear KK relations[20] also predict a reduction of n_2 (quadratic nonlinear index of refraction) for Ar upon single ionization. However, the decrease predicted by KK calculations is less than the one predicted using MCSCF model. The underestimate of the decrease of the nonlinear index of refraction in KK formalism in comparison with the *ab initio* calculations has also been seen for n_2 in other neutral noble gas atoms.[20,65] The discrepancy may be attributed to the use of strong-field ionization rates for the absorption spectra σ_K employed in the KK approach. In addition, the KK integral spans the whole of the frequency axis and thus covers regions where the absorption model used in Ref. [20] is inapplicable.

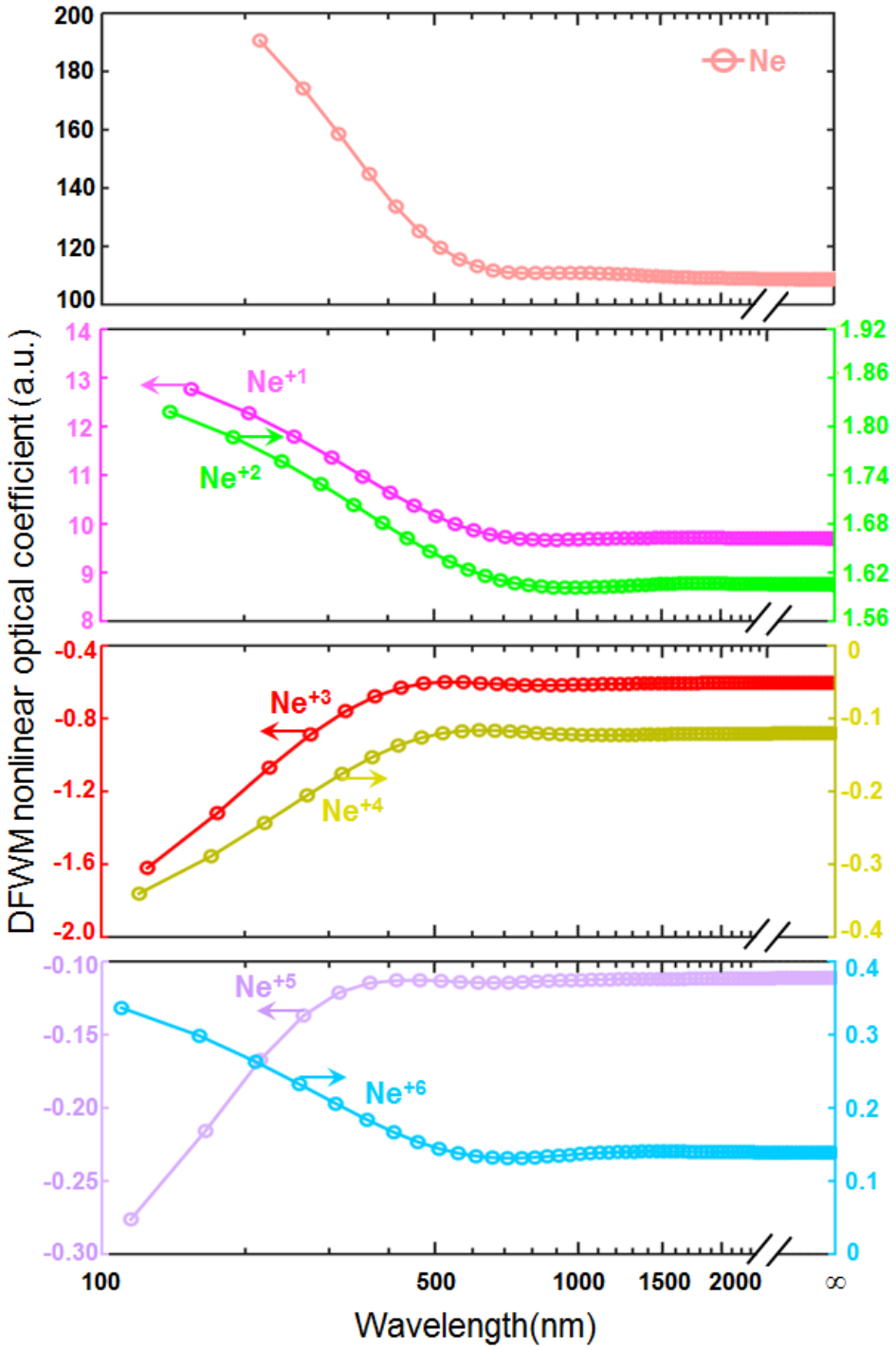

FIG. 9. (Color online) The DFWM coefficient for Ne and multiply charged ions versus wavelength ranging from ~100 nm above the first multi-photon resonance to the static regime. The calculations were performed using CAS (8,12), CAS (5,7), CAS (4,12), CAS (3,12), CAS (4,13), CAS (3,13), and CAS (2,4) for Ne, Ne^{+1}, Ne^{+2}, Ne^{+3}, Ne^{+4}, Ne^{+5}, and Ne^{+6}, respectively. The symmetries used for calculations of Ne, Ne^{+1}, Ne^{+2}, Ne^{+3}, Ne^{+4}, Ne^{+5}, and Ne^{+6} are ^1S_g, ^2P_u, ^3P_g, ^4S_u, ^3P_g, ^2P_u, and ^1S_g, respectively. In all calculations, t-aug-cc-pV5Z basis set was used.

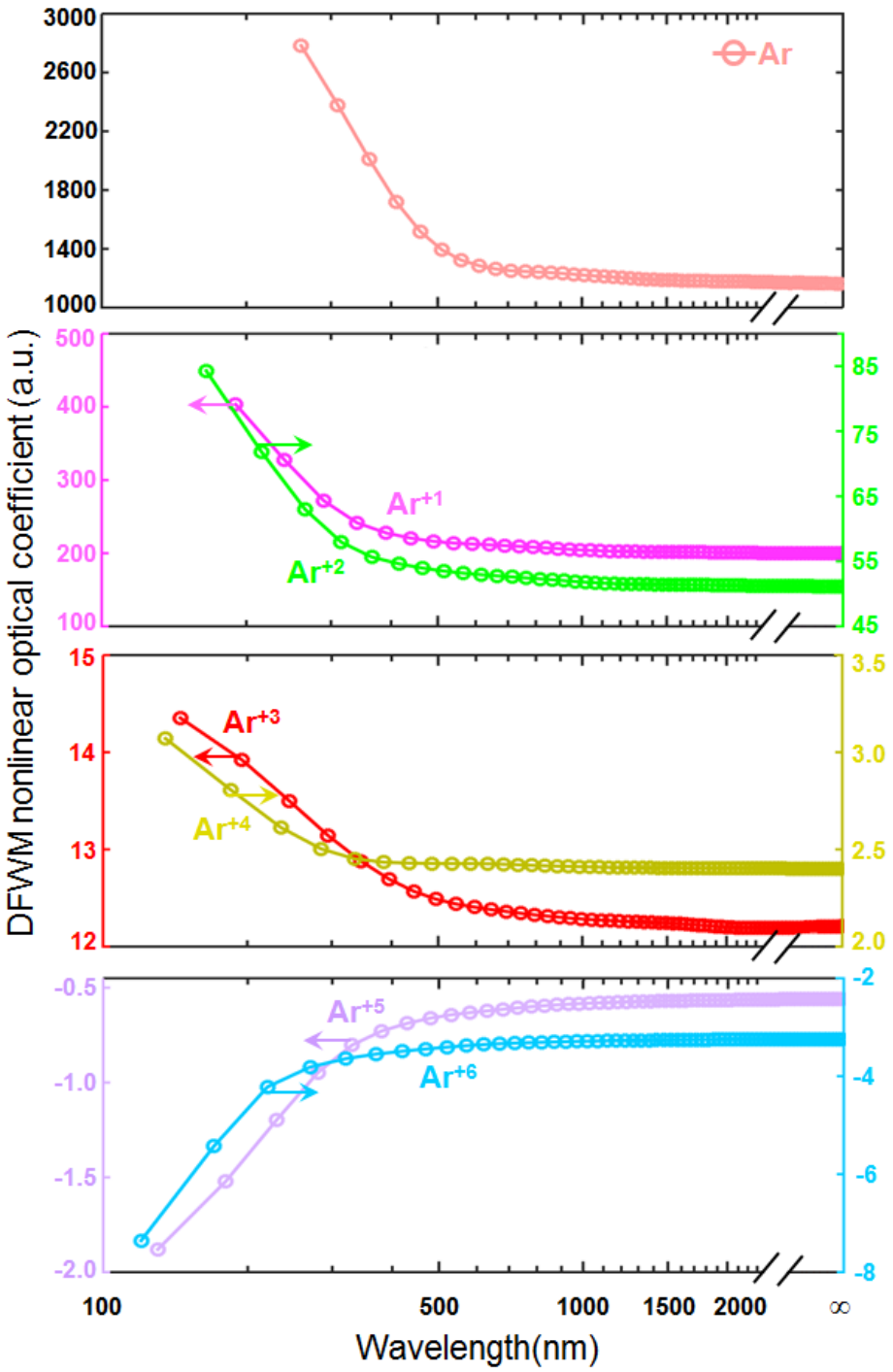

FIG. 10. (Color online) The DFWM coefficient for Ar and multiply charged ions versus wavelength ranging from ~100 nm above the first multi-photon resonance to the static regime. The calculations were performed using CAS (8,14), CAS (7,14), CAS (6,10), CAS (5,13), CAS (4,13), CAS (3,13), and CAS (2,13) for Ar, Ar^{+1}, Ar^{+2}, Ar^{+3}, Ar^{+4}, Ar^{+5}, and Ar^{+6}, respectively. The symmetries used for calculations of Ar, Ar^{+1}, Ar^{+2}, Ar^{+3}, Ar^{+4}, Ar^{+5}, and Ar^{+6} are ^1S_g, ^2P_u, ^3P_g, ^4S_u, ^3P_g, ^2P_u, and ^1S_g, respectively. In all calculations, t-aug-cc-pV5Z basis set was used.

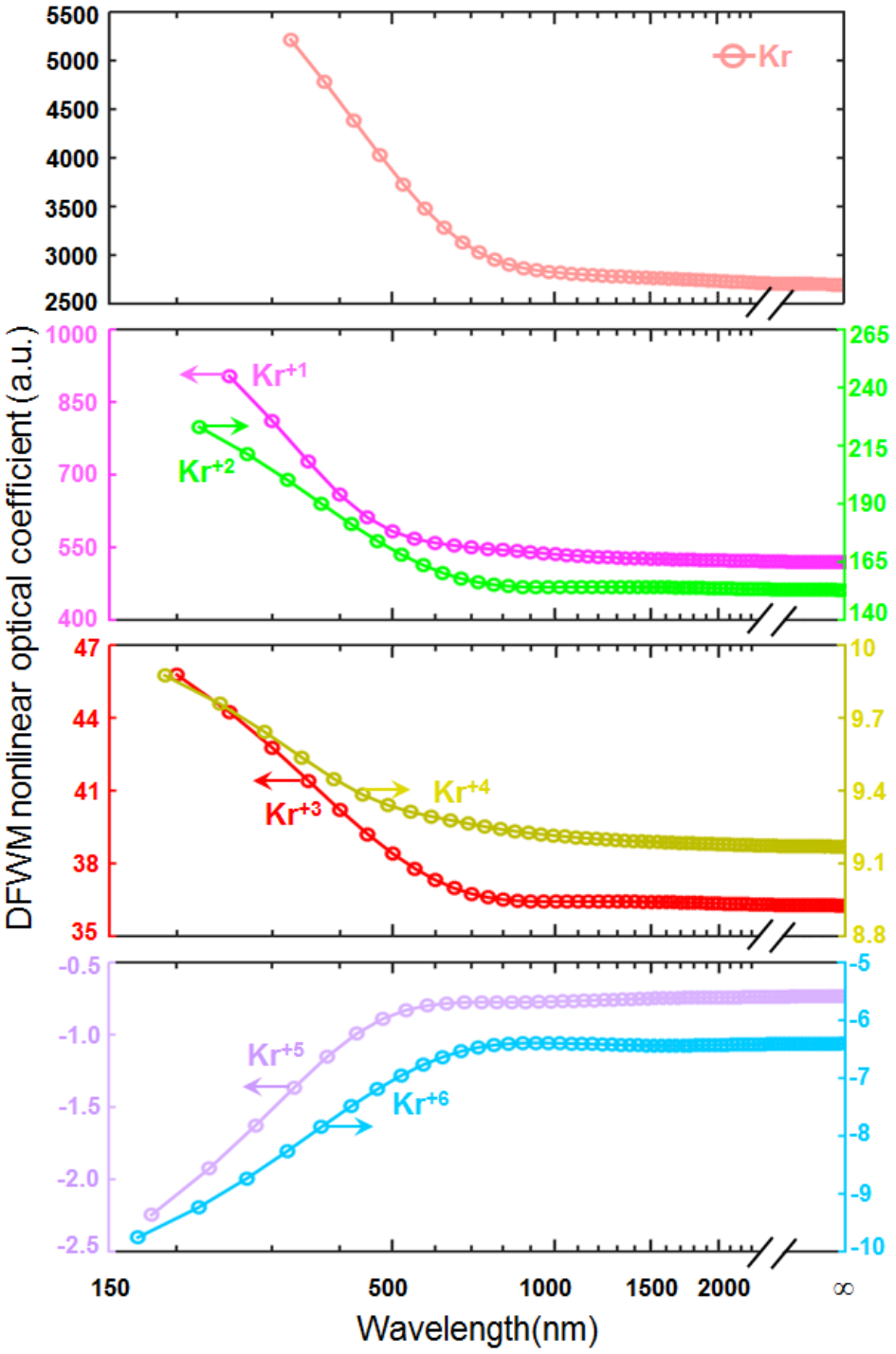

FIG. 11. (Color online) The DFWM coefficient for Kr and multiply charged ions versus wavelength ranging from ~100 nm above the first multi-photon resonance to the static regime. The calculations were performed using CAS (8,13), CAS (7,13), CAS (6,10), CAS (5,10), CAS (4,9), CAS (3,13), and CAS (2,9) for Kr, Kr^{+1}, Kr^{+2}, Kr^{+3}, Kr^{+4}, Kr^{+5}, and Kr^{+6}, respectively. The symmetries used for calculations of Kr, Kr^{+1}, Kr^{+2}, Kr^{+3}, Kr^{+4}, Kr^{+5}, and Kr^{+6} are ^1S_g, ^2P_u, ^3P_g, ^4S_u, ^3P_g, ^2P_u, and ^1S_g, respectively. In all calculations, t-aug-cc-pV5Z basis set was used.

Table II summarizes the computed values of n_2 for noble gases and their multiply charged ions, in the static and high-frequency regime, where all the high-frequency values correspond to wavelengths that are ~100 nm above the two-photon absorption resonance, varying for each species. Comparison of the DFWM coefficients for multiply ionized neon, argon, and krypton, demonstrates the characteristic features similar to that of the helium example. The ratio of n_2 in the frequency dependent regime (the frequencies that are ~0.4557 a.u. below the two-photon absorption resonance) to n_2 in the static regime, $n_2(\omega)/n_2(\omega\to\infty)$,

TABLE II. Nonlinear refractive index n_2 for neutral noble gases and their multiply charged ions, in the static limit, $n_2(\lambda\to\infty)$, and at the shortest wavelength explored, $n_2(\lambda_{\min})$. For each species, $\lambda_{\min}$ is chosen to be ~100 nm above the two-photon absorption resonance. As the multi photon absorption resonance for different atoms/ions varies with ionization potential of the system, the actual values of $\lambda_{\min}$ are different for each ionized species. The n_2 values were calculated using the data in Figs. 8-11 and Eq. 5.

	$n_2(\lambda\to\infty)$ (10^{-9} cm^2/TW)	$n_2(\lambda_{\min})$ (10^{-9} cm^2/TW)
He	3.543	5.962
He^{+1}	0.107	0.138
Ne	8.981	16.307
Ne^{+1}	0.802	1.126
Ne^{+2}	0.132	0.156
Ne^{+3}	-0.049	-0.151
Ne^{+4}	-0.009	-0.033
Ne^{+5}	-0.009	-0.024
Ne^{+6}	0.011	0.034
Ar	96.254	240.679
Ar^{+1}	16.543	34.540
Ar^{+2}	4.234	7.210
Ar^{+3}	1.011	1.188
Ar^{+4}	0.198	0.264
Ar^{+5}	-0.046	-0.156
Ar^{+6}	-0.268	-0.613
Kr	222.775	463.157

kr^{+1}	42.978	75.855
kr^{+2}	12.658	19.220
kr^{+3}	3.001	3.883
kr^{+4}	0.759	0.817
kr^{+5}	-0.060	-0.200
kr^{+6}	-0.530	-0.867

decreases as the ions reach higher ionization potential. Analysis of Figs. 8-11 indicates the quadratic nonlinear Kerr terms as a function of wavelength become less dispersive in higher ionization states. This trend is attributed to the values of IP for the noble gas atoms and the corresponding ionized species. In each sequential ionization stage, the IP value is increased, therefore the multi-photon absorption resonance is reduced and the dispersion of n_2 versus wavelength at higher ionization states decreases.

IV. CONCLUSIONS

An *ab initio,* MCSCF method has been used to calculate the dynamic second-order hyperpolarizability coefficients of atomic noble gases and their positively charged ions for wavelengths ranging from 100 nm to the red of the lowest order multi-photon resonance to the static regime. The calculations of nonlinear response coefficients as a function of active space for each ionized species at 800 nm, demonstrated convergence of the DFWM with different active spaces to within ~5%. For neutral and sextuply ionized species the calculations were also performed at CCSD level. The agreement between the MCSCF- and CCSD-calculated coefficients further validated our methodology for calculation of nonlinear responses of multiply ionized noble gases.

The nonlinear optical responses for multiply ionized noble gases were investigated as a function of state symmetry. The state symmetry effect is most pronounced for Ne ions where the

nonlinear responses of Ne^{+3} and Ne^{+4} in low-spin states change sign in comparison with those in high-spin states. No sign change was observed for triply and quadruply ionized Ar and Kr.

The calculated second-order hyperpolarizability coefficients were used to obtain the dispersions of the quadratic nonlinear index of refraction. The study of second-order nonlinear response coefficients (and/or nonlinear refractive index) versus wavelength, revealed that the magnitude and the dispersion of the nonlinearity decreases when the electrons are progressively removed from the systems. For singly ionized He and Ar noble-gas atoms, the results obtained are in qualitative agreement with Kramers-Kronig based calculations[20].

The results are of value for predictive models of high-harmonic generation in multiply ionized plasma at X-ray photon energies.[8] The results are also pertinent to modeling of femtosecond laser filamentation and especially to nonlinear optical properties of filament wake channels. The predicted modifications of the nonlinear optical response will accompany the changes in linear polarizability of the medium, due to the emergence of free electrons.[23,20] In this capacity, the present calculations are important for developing predictive models for description and control of the filamentation dynamics.

ACKNOWLEDGMENTS

We would like to express our sincere gratitude to Drs. Tenio Popmintchev and Margaret Murnane for fruitful discussion. This work is supported through the Air Force Office of Scientific Research MURI grant FA9550-10-1-0561.

REFERENCES

1. A. Garito and R. F. Shi, Phys. Today **47** (5), 51 (1994).
2. F. Meyers, S. R. Marder, B. M. Pierce and J. L. Bredas, J. Am. Chem. Soc. **116** (23), 10703-10714 (1994).
3. D. S. Watkins and M. G. Kuzyk, J. Chem. Phys. **131** (6), 064110 (2009).

4. M. G. Kuzyk, Phys. Rev. Lett. **85** (6), 1218-1221 (2000).
5. M. G. Kuzyk, J. Pérez-Moreno and S. Shafei, Phys. Rep. **529** (4), 297-398 (2013).
6. P. M. Paul, E. S. Toma, P. Breger, G. Mullot, F. Augé, P. Balcou, H. G. Muller and P. Agostini, Science **292** (5522), 1689-1692 (2001).
7. A. L'Huillier and P. Balcou, Phys. Rev. Lett. **70** (6), 774-777 (1993).
8. D. Popmintchev, C. Hernández-García, F. Dollar, C. Mancuso, J. A. Pérez-Hernández, M.-C. Chen, A. Hankla, X. Gao, B. Shim, A. L. Gaeta, M. Tarazkar, D. A. Romanov, R. J. Levis, et al., Science **350** (6265), 1225-1231 (2015).
9. T. Popmintchev, M. C. Chen, P. Arpin, M. M. Murnane and H. C. Kapteyn, Nat. Photonics **4** (12), 822-832 (2010).
10. P. Béjot, G. Karras, F. Billard, E. Hertz, B. Lavorel, E. Cormier and O. Faucher, Phys. Rev. Lett. **112** (20), 203902 (2014).
11. S. L. Chin, S. A. Hosseini, W. Liu, Q. Luo, F. Théberge, N. Aközbek, A. Becker, V. P. Kandidov, O. G. Kosareva and H. Schroeder, Can. J. Phys. **83** (9), 863-905 (2005).
12. A. Couairon and A. Mysyrowicz, Phys. Rep. **441** (2–4), 47-189 (2007).
13. L. Bergé, S. Skupin, R. Nuter, J. Kasparian and J.-P. Wolf, Rep. Prog. Phys. **70** (10), 1633 (2007).
14. M. Kolesik and J. V. Moloney, Rep. Prog. Phys. **77** (1), 016401 (2014).
15. D. A. Romanov and R. J. Levis, Phys. Rev. E **86** (4), 046408 (2012).
16. R. W. Boyd, *Nonlinear Optics*, Third ed. (Academic Press, San Diego, CA, 2008).
17. M. Kolesik, E. M. Wright and J. V. Moloney, Opt. Lett. **35** (15), 2550-2552 (2010).
18. C. Köhler, R. Guichard, E. Lorin, S. Chelkowski, A. D. Bandrauk, L. Bergé and S. Skupin, Phys. Rev. A **87** (4), 043811 (2013).
19. P. Béjot, E. Cormier, E. Hertz, B. Lavorel, J. Kasparian, J.-P. Wolf and O. Faucher, Phys. Rev. Lett. **110** (4), 043902 (2013).
20. C. Brée, A. Demircan and G. Steinmeyer, Phys. Rev. Lett. **106** (18), 183902 (2011).
21. C. Brée, A. Demircan and G. Steinmeyer, Phys. Rev. A **85** (3), 033806 (2012).
22. P. Polynkin, M. Kolesik, E. M. Wright and J. V. Moloney, Phys. Rev. Lett. **106** (15), 153902 (2011).
23. J. K. Wahlstrand, Y. H. Cheng and H. M. Milchberg, Phys. Rev. Lett. **109** (11), 113904 (2012).
24. J. K. Wahlstrand, Y. H. Cheng, Y. H. Chen and H. M. Milchberg, Phys. Rev. Lett. **107** (10), 103901 (2011).
25. D. L. Weerawarne, X. Gao, A. L. Gaeta and B. Shim, Phys. Rev. Lett. **114** (9), 093901 (2015).
26. M. Tarazkar, D. A. Romanov and R. J. Levis, J. Chem. Phys. **140** (21), 214316 (2014).
27. M. Tarazkar, D. A. Romanov and R. J. Levis, Phys. Rev. A **90** (6), 062514 (2014).
28. M. Tarazkar, D. A. Romanov and R. J. Levis, J. Phys. B: At., Mol. Opt. Phys. **48** (9), 094019 (2015).
29. J. K. Wahlstrand and H. M. Milchberg, Opt. Lett. **36** (19), 3822-3824 (2011).
30. J. H. Odhner, D. A. Romanov, E. T. McCole, J. K. Wahlstrand, H. M. Milchberg and R. J. Levis, Phys. Rev. Lett. **109** (6), 065003 (2012).
31. P. Polynkin, B. Pasenhow, N. Driscoll, M. Scheller, E. M. Wright and J. V. Moloney, Phys. Rev. A **86** (4), 043410 (2012).
32. R. Compton, A. Filin, D. A. Romanov and R. J. Levis, Phys. Rev. Lett. **103** (20), 205001 (2009).

33. R. Compton, A. Filin, D. A. Romanov and R. J. Levis, Phys. Rev. A **83** (5), 053423 (2011).
34. H. Sekino and R. J. Bartlett, J. Chem. Phys. **98** (4), 3022-3037 (1993).
35. O. Christiansen, J. Gauss and J. F. Stanton, Chem. Phys. Lett. **292** (4–6), 437-446 (1998).
36. J. E. Rice, P. R. Taylor, T. J. Lee and J. Almlöf, J. Chem. Phys. **94** (7), 4972-4979 (1991).
37. A. J. Thakkar and A. K. Das, J. Mol. Struc.: THEOCHEM **547** (1–3), 233-238 (2001).
38. M. Sato, A. Kumada and K. Hidaka, Appl. Phys. Lett. **107** (8), 084102 (2015).
39. J. Pipin and D. M. Bishop, Phys. Rev. A **45** (5), 2736-2743 (1992).
40. C. Hättig and P. Jørgensen, J. Chem. Phys. **109** (7), 2762-2778 (1998).
41. S. Høst, P. Jørgensen, A. Köhn, F. Pawłowski, W. Klopper and C. Hättig, J. Chem. Phys. **123** (9), 094303 (2005).
42. C. Neiss and C. Hättig, J. Chem. Phys. **126** (15), - (2007).
43. F. Pawłowski, P. Jørgensen and C. Hättig, Chem. Phys. Lett. **391** (1–3), 27-32 (2004).
44. D. E. Woon and T. H. Dunning, J. Chem. Phys. **100** (4), 2975-2988 (1994).
45. A. K. Wilson, D. E. Woon, K. A. Peterson and T. H. Dunning, J. Chem. Phys. **110** (16), 7667-7676 (1999).
46. K. Aidas, C. Angeli, K. L. Bak, V. Bakken, R. Bast, L. Boman, O. Christiansen, R. Cimiraglia, S. Coriani, P. Dahle, E. K. Dalskov, U. Ekström, T. Enevoldsen, et al., Wiley Interdiscip. Rev.: Comput. Mol. Sci. **4**, 269–284 (2014).
47. C. Hättig, O. Christiansen and P. Jørgensen, Chem. Phys. Lett. **282** (2), 139-146 (1998).
48. A. D. Buckingham, in *Advances in Chemical Physics: Intermolecular Forces*, edited by J. O. Hirschfelder (John Wiley & Sons, Inc., New Jersey, 1967), Vol. 12, pp. 107-142.
49. H. J. A. Jensen, P. Jørgensen, H. Ågren and J. Olsen, J. Chem. Phys. **88** (6), 3834-3839 (1988).
50. S. P. Walch and C. W. Bauschlicher, J. Chem. Phys. **78** (7), 4597-4605 (1983).
51. P. Taylor, in *Lecture Notes in Quantum Chemistry*, edited by B. Roos (Springer, Berlin Heidelberg, 1992), Vol. 58, pp. 89-176.
52. I. N. Levine, *Quantum Chemistry*, Sixth ed. (Prentice-Hall, New Jersey, 2009).
53. J. Olsen and P. Jørgensen, J. Chem. Phys. **82** (7), 3235-3264 (1985).
54. O. Vahtras, H. Ågren, P. Jørgensen, H. J. A. Jensen, T. Helgaker and J. Olsen, J. Chem. Phys. **97** (12), 9178-9187 (1992).
55. T. Helgaker, P. Jørgensen and J. Olsen, *Molecular Electronic-Structure Theory*. (Wiley, New York, 2000).
56. O. Christiansen and P. Jørgensen, Chem. Phys. Lett. **207** (4–6), 367-371 (1993).
57. Y. Luo, O. Vahtras, H. Ågren and P. Jørgensen, Chem. Phys. Lett. **205** (6), 555-562 (1993).
58. D. P. Shelton, Phys. Rev. A **42** (5), 2578-2592 (1990).
59. V. Mizrahi and D. P. Shelton, Phys. Rev. Lett. **55** (7), 696-699 (1985).
60. D. Popmintchev, C. Hernandez-Garcia, B. Shim, M. C. Chen, F. Dollar, C. A. Mancuso, J. Pérez- Hernández, X. Gao, A. Hankla, A. L. Gaeta, M. Tarazkar, D. Romanov, R. Levis, et al., presented at the CLEO: QELS_Fundamental Science, San Jose, California, 2014, FTh5A.9.
61. W. Chen, Z.-R. Li, D. Wu, Y. Li, C.-C. Sun, F. L. Gu and Y. Aoki, J. Am. Chem. Soc. **128** (4), 1072-1073 (2006).
62. H. J. Lehmeier, W. Leupacher and A. Penzkofer, Opt. Commun. **56** (1), 67-72 (1985).
63. S. V. Popruzhenko, V. D. Mur, V. S. Popov and D. Bauer, Phys. Rev. Lett. **101** (19), 193003 (2008).
64. A. M. Perelomov, V. S. Popov and M. V. Terentev, Sov. Phys. JETP **23** (5), 924 (1966).

65. C. Brée, A. Demircan and G. Steinmeyer, IEEE J. Quantum Electron. **46** (4), 433-437 (2010).